

Ultralow-Friction and Ultralow-Wear TiN-Ag Solid Solution Coating in Base Oil

Chang Liu, Xinlei Gu, Lina Yang, Xianqi Song, Mao Wen, Jia Wang, Quan Li, Kan Zhang,*
Weitao Zheng,* and Changfeng Chen*



Cite This: *J. Phys. Chem. Lett.* 2020, 11, 1614–1621



Read Online

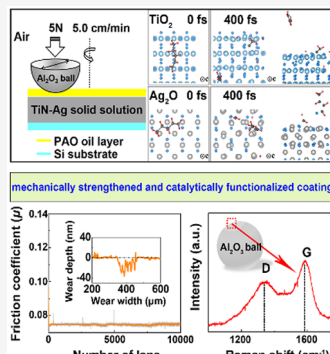
ACCESS |

Metrics & More

Article Recommendations

Supporting Information

ABSTRACT: Lubrication plays a pivotal role in reducing energy consumption and machinery wear, profoundly impacting technological and economic development and the environment. A recent study (Erdemir, A., et al. *Nature* 2016, 536, 67) reported the effective extraction of carbon-based tribofilms from lubricating oil by catalytic activation of the coating material, opening new possibilities for innovative lubrication material research and development. Here, we showcase a solute-atom-strengthened and catalytically functionalized coating design and demonstrate its implementation in a TiN-Ag solid solution film that exhibits concurrent ultralow friction and ultralow wear. Indentation tests and Raman and X-ray photoelectron spectroscopy combined with quantum mechanical simulations uncover the rare superhard nature of the TiN-Ag film along with a solute-Ag-atom-induced self-oxidation mechanism for its outstanding catalytic capacity. These findings identify an outstanding type of mechanically strong and catalytically active coating material with simultaneous superior protective and lubricating functionality, holding great promise for applications ranging from microdevices to large-scale industrial equipment.



Ever-increasing energy consumption and sizable energy losses by moving mechanical assemblies¹ present an urgent challenge to developing clean and efficient lubrication materials for sustainable technological and economic development. Efforts to lower friction and wear by lubrication commonly involve use of antiwear additives like zinc dialkyldithiophosphate (ZDDP),² because base oil without additives often exhibits poor lubricating capacity, especially under harsh conditions.³ However, organic compounds such as ZDDP contain adverse components like sulfated ash, phosphorus, and sulfur, with negative impacts on both the environment and human health.⁴ Better alternatives like ionic liquids and inorganic nanoparticles have been selected to partially or wholly replace ZDDP.^{5–7} It has been suggested that tribochemical layers at moving interfaces can be induced by mechanical shear to improve lubricity. Such tribofilms at interfaces, however, often exhibit poor mechanical properties and can be maintained only when additives are continually supplied, considerably impeding robust applications. Some carbon-based coatings produced low-friction wear debris (lamellar character)^{8–10} at sliding coating surfaces, as seen in metal carbides,^{11,12} and hydrogenated carbon (a-C:H) films,^{13,14} resulting in nanocrystalline graphitic tribofilms with lubricating effects.^{15–17} Graphitic tribofilms also have been seen at metal-on-metal (typically CoCrMo alloys) replacement surfaces *in vivo*, and the carbon source in tribological layers comes from proteins in fluids.^{18,19} This surprising phenomenon is attributed to the catalytic nature of transition metals (Co or Mo) in the implants.²⁰ The tribochemical reaction between

catalysts and organic materials promotes dissociation of the C–H bonds in proteins and C–C bond recombination, thereby extracting graphitic tribofilms. These results offer intriguing insights for effective lubrication through catalytically generating tribofilms at sliding surfaces, but implementation in diverse environments presents major material challenges. Suitable coating materials need to possess concurrent high mechanical strength for durable antiwear function and high catalytic capability for effective lubrication function via self-sustainable tribofilm generation; moreover, the coating fabrication should be robust and versatile for a wide range of practical implementation. A major breakthrough in developing high-performance lubrication coating material was reported in a recent work²¹ that discovered ample carbon-based tribofilms derived from base lubricating oil by a MoN_x-Cu nanocomposite coating. In this case, nanoscale Cu patches embedded in the coating film are exposed at the sliding surface and catalytically active in effectively decomposing base oil molecules and extracting graphitic tribofilms for efficient lubrication while the MoN_x film provides strong antiwear protection. This catalytically active coating design opens new possibilities for innovative lubrication material development.

Received: December 27, 2019

Accepted: February 12, 2020

Published: February 12, 2020

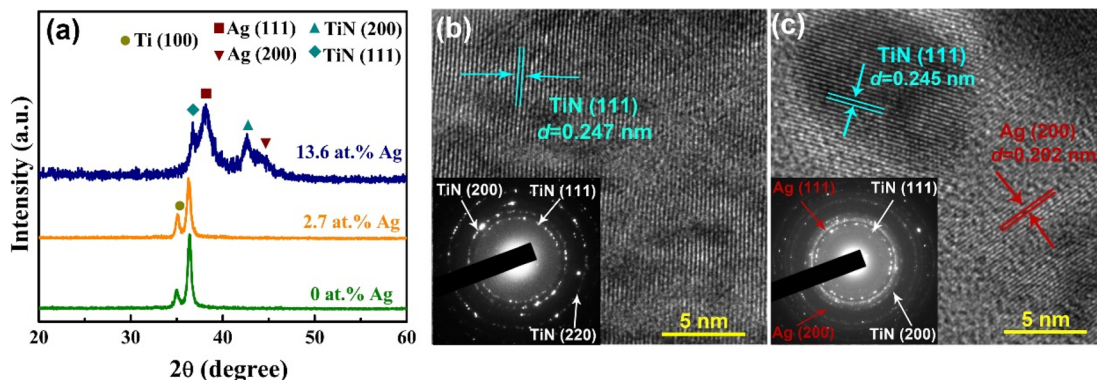


Figure 1. Structure of TiN coatings with different Ag contents. (a) X-ray diffraction (XRD) patterns of TiN coatings with different Ag contents. (b) and (c) HRTEM analysis of the coating with 2.7 and 13.6 atom % Ag.

While $\text{MoN}_x\text{-Cu}$ nanocomposite coating films are reported to be mechanically strong with a hardness of ~ 20 GPa, it is well-known^{22,23} that segregated metal patches embedded in a coating film tend to significantly reduce the mechanical strength of the film, and the film–patch boundaries are especially weak and prone to damage caused by prolonged and repeated loadings. It is therefore crucial for practical applications to find coating materials that possess strong catalytic capability for lubricity and outstanding mechanical strength for durable wear protection.

Here, we report the results of the synthesis and characterization of a newly designed TiN-Ag solid solution coating with outstanding lubricating and protective dual functionalities. Incorporating a relatively low (2.7 atom %) Ag concentration in TiN film leads to the formation of a TiN-Ag solid solution that preserves the TiN crystalline structure and promotes a solute-Ag-induced mechanical strengthening, resulting in a remarkably high indentation hardness near 40 GPa, reaching the superhard category, which is rare among transition-metal compounds. The film has an ultralow wear rate of 5.56×10^{-11} mm³/Nm. Moreover, the solute-Ag atoms induce self-oxidation at the coating surface, producing strong catalytic capability for extracting graphitic tribofilms from the base lubricating oil, leading to ultralow friction coefficients of 0.075 at loads of 5.0 N. In sharp contrast, at a higher concentration (13.6 atom %), Ag atoms form precipitated patches at the surface, similar to Cu patches in $\text{MoN}_x\text{-Cu}$ films;²¹ this coating produces ultralow friction stemming from the Ag patch-induced catalytic capability, but it is mechanically much weaker, with a hardness of only 10.6 ± 2.3 GPa, due to the presence of Ag precipitates. The concurrent ultralow friction and ultralow wear of the TiN-Ag solid solution coating showcase the promise of solute-atom-strengthened and catalytically functionalized coating design and implementation for a wide range of applications. Our results are expected to stimulate further research leading to discovery of more coating materials that exhibit concurrent superior lubrication and protection capabilities.

We deposited TiN coatings on a Si substrate using magnetron sputtering under a high substrate bias voltage in mixed discharge gases of Ar and N₂ and introduced Ag atoms into the TiN film by magnetron co-sputtering individual Ti and Ag targets (see **Methods in the Supporting Information** for more details). On the basis of X-ray photoelectron spectroscopy (XPS) results after surface etching, the compositions of all samples were obtained from the relative intensities of the Ti

2p, N 1s, and Ag 3d XPS peaks. The measured composition of each sample deposited using different powers on Ag is summarized in **Table S1**. Two representative Ag-containing TiN coatings are determined to host 2.7 and 13.6 atom % Ag, respectively, in the low- and high-Ag concentration regime. Structural analysis was carried out by X-ray diffraction (XRD) and transmission electron microscopy (TEM) analyses. XRD patterns (**Figure 1a**) reveal structural variations with a change in Ag content. For the pure TiN coating, a face center cubic (*fcc*) structure with the (111) orientation is confirmed by referencing PDF Card 65-0715. A weak peak at a diffraction angle of 35.02° is designated using PDF Card 65-9622 as a peak of Ti, stemming from the layer between the coating and Si substrate. The *fcc* structure remains intact when 2.7 atom % Ag is added, as evidenced by a lack of new XRD peaks associated with any Ag phase, indicating the successful synthesis of a single-phase TiN-Ag solid solution coating. Meanwhile, the calculated formation enthalpies (ΔH) of pure TiN and a TiN-Ag solid solution are -1.692 and -1.472 eV/atom (**Table S1**), respectively, confirming that both TiN and TiN-Ag solid solution structures are energetically stable. A higher Ag content (13.6 atom %) results in segregated Ag clusters precipitating in the TiN lattice forming the TiN/Ag nanocomposite coating, as evidenced by the appearance of an obvious Ag phase revealed by its (111) and (200) peaks (PDF Card 65-0715).

To further identify the structural features of the coatings with 2.7 and 13.6 atom % Ag, we show in panels b and c of **Figure 1** the corresponding TEM results with selected area electron diffraction (SAED) patterns. Here, the pure TiN diffraction ring and large-area TiN(111) plane can be detected in the case of 2.7 atom % Ag, confirming the formation of a TiN-Ag solid solution, while the coating containing 13.6 atom % Ag shows a mixed diffraction ring composed of both the TiN phase and the Ag phase. Moreover, Ag grains with an interplanar spacing of 0.236 nm are observed in the high-resolution TEM (HRTEM) image, demonstrating the presence of the segregated Ag phase coexisting with the TiN phase. Three-dimensional (3D) atomic force microscopy images give further evidence of precipitated Ag nanoclusters at the coating surface, because a roughness much higher than those of other coatings is present in this case (**Figure S1**). The analysis described above identifies two types of Ag atoms in TiN coatings; one type consists of the solute Ag atoms in the TiN-Ag substitutional solid solution (2.7 atom % Ag), and the other

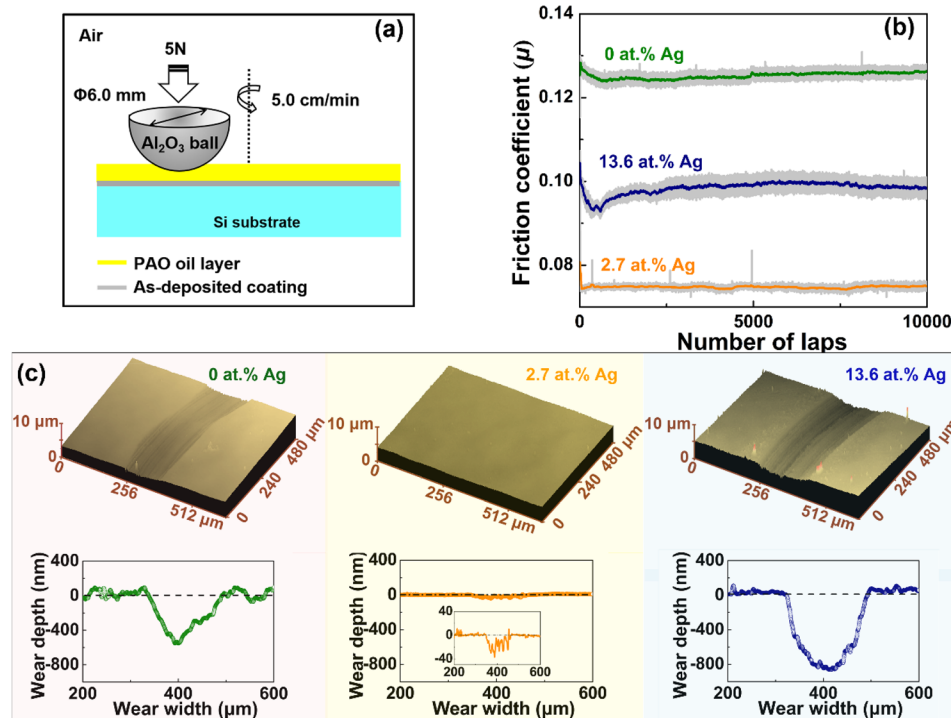


Figure 2. Friction and wear behavior of the of the TiN coating with different Ag contents in PAO10 oil. (a) Schematic diagram of the friction test equipment with the ball-on-disk rotating mode. (b) Measured friction coefficient μ vs the number of cycles during the sliding of an Al₂O₃ ball on each sample in PAO10 oil. (c) Three-dimensional images and line scans showing the extent of wear damage.

type is the TiN/Ag nanocomposite structure coating with precipitated Ag nanoclusters (13.6 atom % Ag).

To understand the role of different amounts and forms of Ag content in TiN-Ag coatings in influencing tribological behavior in base lubricating oil, we have measured the friction coefficient (μ) using the setup and process depicted in Figure 2a. The obtained μ values are shown in Figure 2b. It is seen that for a pure TiN coating μ remains stable at ~ 0.125 , in the range of typical values for PAO-lubricated sliding contacts ($\mu \sim 0.13\text{--}0.15$).^{24,25} The μ values drop to an ultralow value of 0.075 at the same load for the coating with 2.7 atom % Ag, representing a 40% reduction compared to that of the Ag-free pure TiN coating. For the coating with 13.6 atom % Ag that hosts Ag grains segregated from the TiN lattice, μ values stay around 0.099. To explore the underlying mechanism for the variation of the measured μ values, the wear tracks for each sample were ultrasonically cleaned in an acetone solution and then observed with a 3D laser confocal scanning microscope. The micrographs in Figure 2c indicate that the Ag-free coating shows a relatively wide wear track with deep ravines, indicating serious wear loss due to friction with the counterpart ball. In sharp contrast, smooth surfaces without discernible grooving are seen in the wear track of the TiN-Ag solid solution coating containing 2.7 atom % Ag. At 13.6 atom % Ag, the coating exhibits a much deeper wear track with darker regions. The extent of wear damage for the samples can be also observed directly by SEM micrographs and SEM-EDS mapping images (Figure S2). We performed a quantitative comparison of wear rates for different coatings. The cross sections of worn profiles show that the pure TiN coating is wider and deeper than that in the TiN-Ag solid solution coating with 2.7 atom % Ag, with corresponding wear rates of 1.35×10^{-9} and 5.56×10^{-11} mm³/Nm, respectively. Meanwhile, the TiN-Ag coating with 13.6 atom % Ag containing precipitated Ag clusters shows the

highest wear rate of 2.07×10^{-9} mm³/Nm, which is considerably worse compared to those of the TiN and TiN-Ag solid solution film. Furthermore, we have prolonged the sliding cycles to 30000 for the TiN-Ag solid solution film. The low and stable friction coefficient and the smooth wear trace indicate that the TiN-Ag solid solution film is robust and durable (see Figure S3), which may be attributed to the compression-shear loading condition in the wearing process, which may have hindered potentially brittle deformation modes.²⁶ For reference, we also ran tests on an unprotected Si substrate and obtained an unsteady friction coefficient and a much higher wear rate of 1.04×10^{-7} mm³/Nm under the same condition (Figure S4).

We performed indentation measurements on the three coating films. Hardness values were taken in the impression depth range of 100–200 nm for all samples (Figure S5). The pure TiN coating exhibits a high hardness of 33.9 ± 2.2 GPa, which is attributed to the strong Ti–N bonding that is further enhanced by the compressive stress [5.16 GPa (Table S1)] introduced by the substrate bias.²⁷ The incorporation of 2.7 atom % solute Ag atoms into the TiN lattice hardens the resulting solid solution, which exhibits a hardness of 39.6 ± 3.1 GPa, making the TiN-Ag solid solution coating reach the superhard category,²⁸ which is rare among transition-metal compounds. This remarkable nearly 20% enhancement in hardness over the result for the original TiN film likely stems from the immobilization of dislocations by the inhomogeneous local stress fields introduced by solute-Ag atoms in an intrinsically already very hard TiN film. Increasing the Ag content to 13.6 atom % produces precipitated Ag clusters that are very soft, and the coating hardness drastically decreases to 10.6 ± 2.3 GPa. These contrasting hardness data explain the large variations in wear rate presented above. The elastic modulus exhibits a composition dependence similar to that of

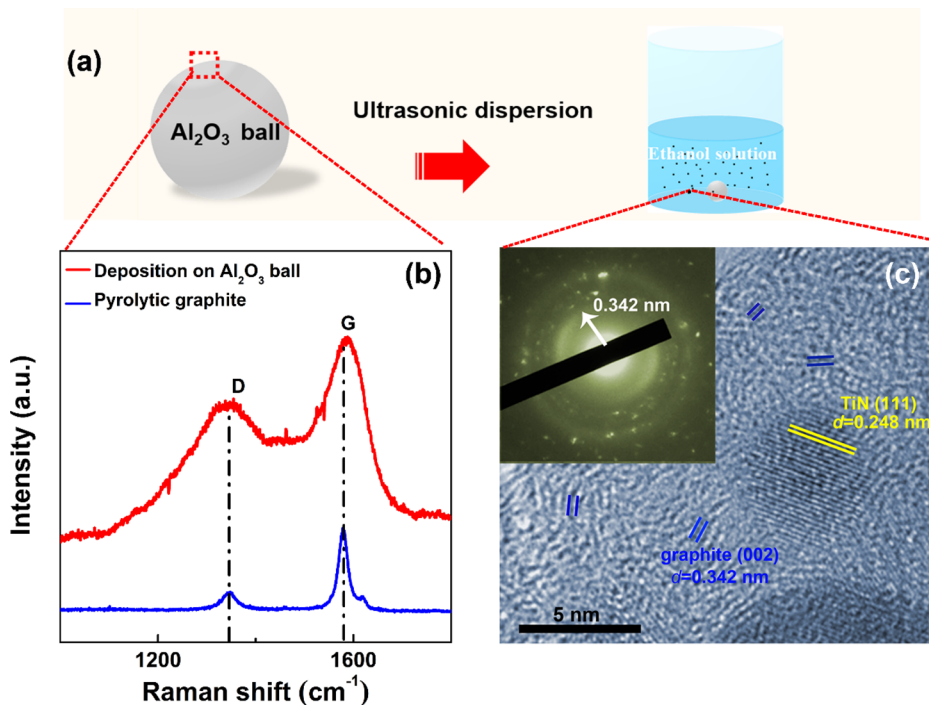


Figure 3. Characterization of wear debris of a rubbing ball with the TiN-Ag solid solution coating after the friction test. (a) Schematic diagram of the area around the wear scar on an Al₂O₃ ball. The debris around the wear scar of the sliding ball was analyzed by Raman spectroscopy; meanwhile, the debris was also collected by ultrasonic dispersion of the sliding ball in an acetone solution and then characterized by TEM. (b) Raman spectra of wear debris from the counterpart ball produced during its siding over the TiN-Ag solid solution coating in a PAO oil environment and Raman spectra of pyrolytic graphite also shown as a reference. (c) TEM image of wear debris from the sliding ball.

H , increasing from $E = 309.8 \pm 9.0$ GPa for pure TiN to a maximum of $E = 314.5 \pm 6.5$ GPa for the TiN-Ag solid solution and a subsequent decrease to 119.6 ± 10.8 GPa for the TiN/Ag nanocomposite coating. These contrasting mechanical data explain the large variations in wear rate presented above. Meanwhile, the difference in the friction products, i.e., presence or absence and nature of wear debris, holds the key to understanding the large contrast of tribological behaviors for pure TiN and TiN-Ag solid solution coatings, because they exhibit similar hardnesses but significantly different μ values.

To understand the ultralow-friction and ultralow-wear nature of the TiN-Ag solid solution coating, Raman and TEM measurements were conducted on the debris around the wear scar of the sliding ball to reveal its chemical and structural nature. The debris from the wear scar on the rubbing ball was directly detected by Raman spectroscopy and then collected by ultrasonic dispersion in an acetone solution to be analyzed by TEM (Figure 3a). The obtained Raman spectrum shown in Figure 3b split into two Gaussian peaks centered at around 1336 and 1586 cm⁻¹, which are assigned to well-defined D and G peaks, respectively.²⁹ Note that the D peak corresponds to the breathing vibration of disordered sp²-hybridized carbon while the G peak corresponds to the stretching mode of sp² bonding,³⁰ and the relative intensity of the D peak and G peak (I_D/I_G) reflects the degree of graphitization. Here, the I_D/I_G value for the resulting wear debris is 0.72, allowing an estimate of nanographite size (L_a) of ~ 6.2 nm according to a linear relation.¹⁸ The TEM results (Figure 3c) taken at the debris edge that is electron transparent reveal a large-area ordered region with typical nanostructures of short curved or parallel clustered plane stacks. The fringe spacing was measured to be ~ 0.342 nm, suggesting that the tribological layer is primarily

graphitized carbon.¹⁹ The presence of some embedded nanoclusters can be assigned to TiN grains on the basis of their interplanar spacing at 0.243 nm. The inset shows a typical diffraction pattern of the graphitic material with a dominant spacing of ~ 0.342 nm, corroborating the HRTEM observation. In addition, the wear debris from the rubbing ball of the pure TiN coating and TiN with a 13.6% Ag coating were also characterized by Raman spectroscopy (Figure S6). No signal was observed for the TiN coating, while D and G peaks are clearly seen for the TiN/Ag nanocomposite coating, similar to the results for the TiN-Ag solid solution coating. The lack of graphitic tribofilm for the TiN coating explains its highest μ values.

The Raman and TEM results show that tribochemical reaction between the TiN-Ag solid solution coating and base lubricating oil produces a graphitic material leading to the observed ultralow friction, which is similar to the result for previously reported carbon-based tribofilms extracted from lubricating oil by MoN_x-Cu coatings, where Cu patches at coating surfaces act as a catalytic agent.²¹ Here, the superhard character of the TiN-Ag solid solution coating film represents a considerably improved high-performance mechanical feature that produces the concurrently measured ultralow wear rate.

We now turn to the mechanism underlying the catalytic effects that are responsible for extracting graphitic tribofilms from base lubricating oil by the TiN-Ag solid solution coating. We examine the role of solute Ag atoms in effecting structural and chemical changes that facilitate catalytically promoted breakdown of the base oil molecules as a precursor to the formation of tribofilms, as recently seen in the MoN_x-Cu-induced process.²¹ Our results indicate that solute Ag atoms play a decisive role in promoting catalytic behavior because a pure TiN coating exhibits a greatly reduced catalytic activity as

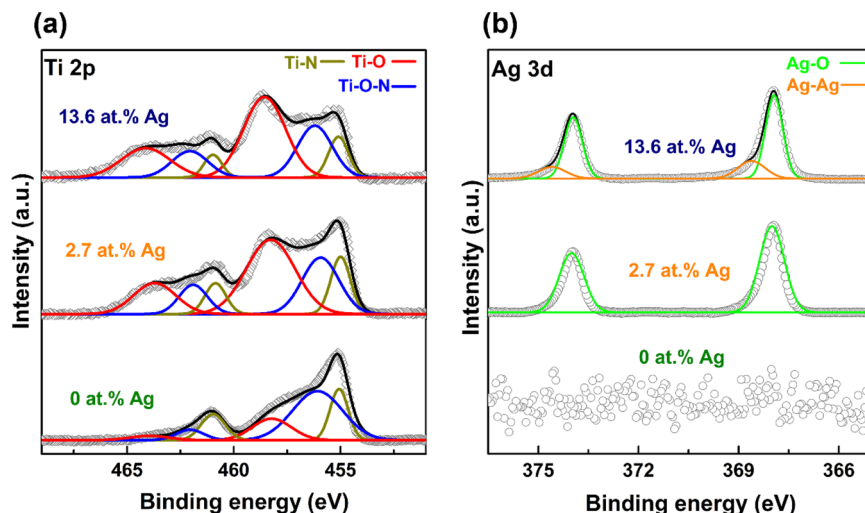


Figure 4. X-ray photoelectron spectroscopy probing of the surface chemistry of the TiN coating with different Ag contents. (a) High-resolution spectra showing the peaks corresponding to Ti 2p orbitals for the three samples. (b) High-resolution spectra showing Ag 3d orbitals.

evidenced by the elevated friction coefficient (Figure 2b), indicating a lack of catalytically generated carbon-based tribofilms, which is consistent with the observation that a pure MoN coating also has low catalytic activity.²¹ The coating surface where tribochemical reaction occurs is of primary interest.³¹ We performed XPS measurements to probe Ti 2p and Ag 3d core level spectra for the surface of each sample. The pure TiN coating shows partial oxidation, as evidenced by the simultaneous presence of Ti–N, Ti–O, and Ti–O–N bonds (Figure 4a). However, the formation of Ti⁺ and N^{3−} on the surface of the coating lowers the valence DOS and makes the surface of TiN chemically inert.^{32,33} Solute Ag atoms induce a large increase in the number of Ti–O bonds, forming the mass of TiO₂ on the surface.³⁴ The Ag 3d spectra (Figure 4b) show oxidation states corresponding to the Ag₂O peak centered around 367.7 and 373.5 eV. With a further increase in Ag content, precipitation of Ag leads to coexisting Ag₂O and Ag nanoclusters (Ag–Ag bonds at 368.4 and 374.3 eV).³⁵ These results show clearly that solute Ag atoms promote self-oxidation of the TiN–Ag solid solution coating surface, producing TiO₂ and Ag₂O that coexist on the TiN–Ag film surface. Moreover, solute Ag atoms with fewer valence electrons are expected to lead to charge depletion on neighboring Ti atoms, making these Ti atoms undercoordinated, which would further promote self-oxidation of the TiN–Ag coating exposed to air. We have checked the TiN–Ag solid solution coating for its surface wettability, and our results offer evidence of the formation of Ag₂O clusters at the surface because the Ag⁺ ions in Ag₂O are coordinate-saturated with a filled-shell (4d¹⁰5s⁰) structure, which inhibits the hydrogen-bonding network with interfacial water molecules to achieve ultrahigh hydrophobicity (Figure S7).^{36,37}

To elucidate the experimentally observed capability of the TiN–Ag solid solution coating in generating carbon-based tribofilms for ultralow friction, we have performed quantum mechanical simulations to assess the catalytic functionality of pertinent materials present in the coating film by the original synthesis and self-oxidation process, including Ag metal, and TiN, TiO₂, and Ag₂O compounds. It was shown in a recent work²¹ that Cu patches embedded in the MoN_x–Cu film can effectively decompose hydrocarbon molecules in base lubricating oil, leading to the formation of graphitic tribofilms that

produce ultralow friction. Here we employ ab initio molecular dynamics (AIMD) simulations to examine the catalytic action of the Ag surface. The results in Figure 5a show that the Ag surface also exhibits the ability to dehydrogenate and break linear olefins into shorter-chain hydrocarbons, which is a key prerequisite for generating carbon-based tribofilms.²¹ Meanwhile, results in Figure 5b show that olefins also break up on the TiN surface, but the resulting carbon atoms tend to react and bond with Ti and, thus, are no longer able to form graphitic structures or impede further decomposition of oil molecules because the surface Ti sites become increasingly catalytically inactive due to their bonding with the carbon atoms, similar to the situation previously observed on the MoN_x surface.²¹ These results showcase the crucial role of Ag patches in generating the substantial catalytic capability observed in the TiN–Ag film containing a high (13.6 atom %) concentration of Ag, comparable to the case of the MoN_x–Cu film, where Cu patches act as the catalytic sites. A distinct feature of the TiN–Ag solid solution film is the solute-Ag-atom-promoted self-oxidation at the film surface. While the exact morphologies of the resulting Ti and Ag oxides are unknown, we examined the catalytic process on TiO₂ and Ag₂O surfaces using AIMD simulations. The results in panels c and d of Figure 5 show that these two surfaces possess the same catalytic capability to break up and dehydrogenate the oil molecules, resulting in short carbon units that serve as the building blocks in forming graphitic tribofilms.²¹ To corroborate simulation results, we measured the friction character of pure TiO₂ and Ag₂O coatings by the ball-on-disk test and obtained consistently low friction coefficients of 0.05 and 0.07, respectively, at loads of 1.0 N necessitated by the softness of these coatings. Meanwhile, the resulting wear debris at the sliding contact interface shows clear signals of D and G bands in Raman spectra (Figure S8), indicating the presence of a graphitic tribofilm in agreement with the results of the AIMD simulations.

Our AIMD simulations and analysis show a compelling scenario for *in situ* formation of graphitic tribofilms by dissociative extraction from base lubricating oil by TiN–Ag solid solution coating. This process begins with the activation of the C–H bonds by the Ag₂O/TiO₂ composites at the coating surface that are in good contact with oil molecules.

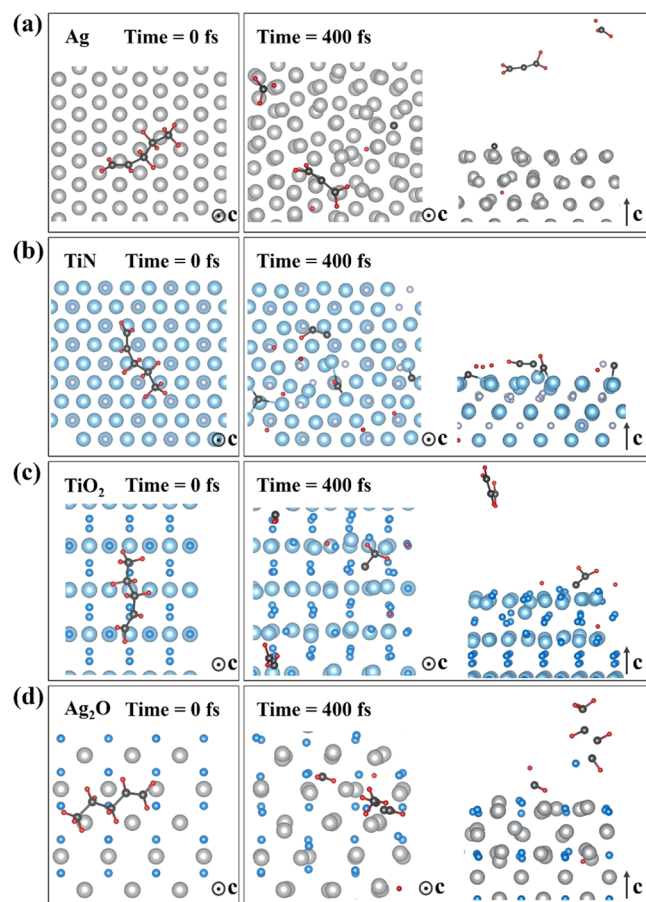


Figure 5. Catalytic action of (a) Ag, (b) TiN, (c) TiO_2 , and (d) Ag_2O illustrated by AIMD simulations. A linear olefin molecule is randomly placed on one of the four surfaces studied in this work. AIMD simulations were run at a constant temperature of 1000 K, and at the end of the 400 fs simulation, the olefin molecule is shown to be dehydrogenated and broken into shorter-chain hydrocarbons on the four different surfaces. Most of the broken hydrocarbons escape from the Ag, TiO_2 , and Ag_2O surface, and these free short-chain hydrocarbons can form graphitic tribofilms under practical loading conditions.²⁶ Meanwhile, all carbon atoms stay close to and bond with Ti atoms on the TiN surface, impeding further catalytic processes.

Such multimetal oxides are known to be effective for catalytic dehydrogenation,^{38,39} and $\text{Ag}_2\text{O}(\text{Ag})/\text{TiO}_2$ -based heterojunctions have led to enhanced catalytic activity for methylene blue dye degradation based on better electron/hole separation.^{40,41} Here, high contact pressure or shear stress generated heat⁴² would promote catalytic events by lowering the activation energy for dissociative extraction of graphitic tribofilms from hydrocarbon molecules in lubricating oils.²¹ Once these surface composites are worn into smaller particles and completely immersed in oil, their contacting areas with oil molecular chains are enhanced, leading to higher catalytic efficiency. Meanwhile, during the continuous oxidation of such solid solution coatings, electron transfer occurs from the TiN-Ag coating material to oil molecule chains, further facilitating the dehydrogenation of hydrocarbons and recombination to form carbon-based tribofilms, because charge transfer events between catalyst surfaces and PAO molecule chains govern their catalytic actions.^{43,44} Consequently, a combination of lubricating oil and solid graphitic tribofilms provides a highly favorable sliding interface, which together with the superhard

nature of the coating produces simultaneously ultralow friction and ultralow wear. Solid solution materials offer an appealing design rationale for their ability to achieve solute-enhanced mechanical strengthening⁴⁵ and catalytic reactivity.⁴⁶ Solute Ag atoms in transition-metal nitrides have shown a self-oxidation capacity in generating metallic oxides^{47,48} with good catalytic activity.^{49–52} This work highlights the TiN-Ag solid solution film as a key case of these design principles in generating outstanding concurrent lubrication and protective functionalities, which may stimulate research leading to further discoveries of robust and high-performance coatings.

We have introduced and implemented in this work a newly designed, synthesized, and characterized solute-atom-strengthened and functionalized superhard coating material. The obtained coating exhibits superior mechanical strength and effective catalytic capacity in generating graphitic tribofilms from the environmentally friendly base oil without any additives, leading to simultaneous ultralow-friction and ultralow-wear performance. Our results showcase the crucial role of solute-atom-enabled self-oxidation in promoting the active catalytic reaction for tribological applications. The synthesized TiN-Ag solid solution film possesses concurrent high catalytic capability and superhard mechanical character, representing a distinct type of superior lubricating material that can be readily adopted in a wide range of device and machinery settings for operation in diverse environments. A key feature in coating functionalization is the surface self-oxidation that, aided by contact pressure or shear generated heat, promotes effective extraction of graphitic tribofilms from base oil molecules. This intrinsic catalytic behavior provides a constant supply of highly efficient lubricating agents, ensuring robust catalytic events and self-replenishing production of graphitic tribofilms. The superhard solid solution-enhanced catalytic coating design and its successful implementation demonstrate a promising approach to developing advanced lubrication materials that hold great promise for fuel-efficient, wear-resistant, and greener energy consumption technology. This work raises exciting prospects of developing additional high-performance lubrication coating materials in a large class of solute-atom-enhanced transition-metal compounds, possibly beyond the currently studied nitride series.

In summary, we present a new design of mechanically strengthened and catalytically functionalized coating and demonstrate its implementation in a TiN-Ag solid solution film that exhibits concurrent ultralow friction and ultralow wear. Such carbon-based tribofilms can form in operando via dissociative extraction from base oil molecules on catalytically active coating surfaces without any additives, enabling base oils to provide both lubricating fluid and solid tribofilms. Indentation tests and Raman and X-ray photoelectron spectroscopy combined with quantum mechanical simulations uncover the rare superhard nature of the TiN-Ag film along with a solute-Ag-atom-induced self-oxidation mechanism for its outstanding catalytic capacity. These findings merge superior features in tribology and catalysis, holding promise for further discovery and development of distinct advanced lubrication and protection materials.

ASSOCIATED CONTENT

SI Supporting Information

The Supporting Information is available free of charge at <https://pubs.acs.org/doi/10.1021/acs.jpcllett.9b03864>.

Detailed experimental and simulation methods; one table of the composition contents, hardnesses, elastic moduli, intrinsic stresses, and calculated enthalpies of formation [ΔH (electronvolts per atom)] for different samples; and eight figures showing the roughness of different samples, SEM and mapping pictures for wear traces of all samples, the friction coefficient and wear trace of the TiN-Ag solid solution coating when the number of sliding cycles is increased to 30000, the friction coefficient and wear rate of pure silicon, the hardness as a function of indentation depth, the Raman signal of friction debris on the Al_2O_3 ball, the water contact angles of all samples, and the EDS, friction coefficient, and Raman spectra for Ag_2O and TiO_2 films (PDF)

AUTHOR INFORMATION

Corresponding Authors

Kan Zhang – State Key Laboratory of Superhard Materials, Department of Materials Science and Key Laboratory of Automobile Materials, MOE, Jilin University, Changchun 130012, China;  orcid.org/0000-0003-1354-2784; Email: kanzhang@jlu.edu.cn

Weitao Zheng – State Key Laboratory of Superhard Materials, Department of Materials Science and Key Laboratory of Automobile Materials, MOE, Jilin University, Changchun 130012, China; Email: wtzheng@jlu.edu.cn

Changfeng Chen – Department of Physics and Astronomy, University of Nevada, Las Vegas, Nevada 89154, United States; Email: chen@physics.unlv.edu

Authors

Chang Liu – State Key Laboratory of Superhard Materials, Department of Materials Science and Key Laboratory of Automobile Materials, MOE, Jilin University, Changchun 130012, China

Xinlei Gu – State Key Laboratory of Superhard Materials, Department of Materials Science and Key Laboratory of Automobile Materials, MOE, Jilin University, Changchun 130012, China

Lina Yang – State Key Laboratory of Superhard Materials, Department of Materials Science and Key Laboratory of Automobile Materials, MOE, Jilin University, Changchun 130012, China

Xianqi Song – State Key Laboratory of Superhard Materials, Department of Materials Science and Key Laboratory of Automobile Materials, MOE, Jilin University, Changchun 130012, China

Mao Wen – State Key Laboratory of Superhard Materials, Department of Materials Science and Key Laboratory of Automobile Materials, MOE, Jilin University, Changchun 130012, China;  orcid.org/0000-0002-6288-4628

Jia Wang – State Key Laboratory of Superhard Materials, Department of Materials Science and Key Laboratory of Automobile Materials, MOE, Jilin University, Changchun 130012, China

Quan Li – State Key Laboratory of Superhard Materials, Department of Materials Science and Key Laboratory of Automobile Materials, MOE, Jilin University, Changchun 130012, China;  orcid.org/0000-0002-7724-1289

Complete contact information is available at:
<https://pubs.acs.org/10.1021/acs.jpcllett.9b03864>

Author Contributions

C.L. and X.G. contributed equally. K.Z. designed the project and directed the experiments. C.C. supervised the theoretical efforts. C.L. carried out most computational modeling and simulation tasks and the associated data processing and analysis. X.G. performed most experiments. L.Y., X.S., M.W., and J.W. assisted with measurements and computations. C.L., X.G., L.Y., X.S., M.W., J.W., Q.L., K.Z., W.Z., and C.C. contributed to analysis and discussion of results. K.Z., X.G., C.L., and C.C. wrote the paper with input from all authors.

Notes

The authors declare no competing financial interest.

ACKNOWLEDGMENTS

This work was supported by the National Natural Science Foundation of China (Grants 51972139, 51602122, 51871109, and 51905206), the National Key R&D Program of China (Grant 2016YFA0200400), the China Postdoctoral Science Foundation (Grant 2017T100207), the Program for JLJU Science and Technology Innovative Research Team (2017TD-09), and the Fundamental Research Funds for the Central Universities.

REFERENCES

- (1) Chu, S.; Majumdar, A. Opportunities and Challenges for a Sustainable Energy Future. *Nature* **2012**, *488*, 294.
- (2) Gosvami, N. N.; Bares, J. A.; Mangolini, F.; Konicek, A. R.; Yablon, D. G.; Carpick, R. W. Mechanisms of Antiwear Tribofilm Growth Revealed in situ by Single-Asperity Sliding Contacts. *Science* **2015**, *348*, 102–106.
- (3) Rodriguez Ripoll, M.; Tomala, A.; Gabler, C.; DraZic, G.; Pirker, L.; Remskar, M. In situ Tribocorrosion of Molybdenum Oxide Nanotubes. *Nanoscale* **2018**, *10*, 3281–3290.
- (4) Michael Cisson, C.; Rausina, G. A.; Stonebraker, P. M. Human Health and Environmental Hazard Characterisation of Lubricating Oil Additives. *Lubr. Sci.* **1996**, *8*, 145–177.
- (5) Jaiswal, V.; Rastogi, R. B.; Kumar, R.; Singh, L.; Mandal, K. D. Tribological Studies of Stearic Acid-Modified $\text{CaCu}_{2.9}\text{Zn}_{0.1}\text{Ti}_4\text{O}_{12}$ Nanoparticles as Effective Zero Saps Antiwear Lubricant Additives in Paraffin Oil. *J. Mater. Chem. A* **2014**, *2*, 375–386.
- (6) Qu, J.; Barnhill, W. C.; Luo, H.; Meyer, H. M., Iii; Leonard, D. N.; Landauer, A. K.; Kheireddin, B.; Gao, H.; Papke, B. L.; Dai, S. Synergistic Effects between Phosphonium-Alkylphosphate Ionic Liquids and Zinc Dialkyldithiophosphate (ZDDP) as Lubricant Additives. *Adv. Mater.* **2015**, *27*, 4767–4774.
- (7) Guo, W.; Zhou, Y.; Sang, X.; Leonard, D. N.; Qu, J.; Poplawsky, J. D. Atom Probe Tomography Unveils Formation Mechanisms of Wear-Protective Tribofilms by ZDDP, Ionic Liquid, and Their Combination. *ACS Appl. Mater. Interfaces* **2017**, *9*, 23152–23163.
- (8) Erdemir, A.; Donnet, C. Tribology of Diamond-Like Carbon Films: Recent Progress and Future Prospects. *J. Phys. D: Appl. Phys.* **2006**, *39*, R311–R327.
- (9) Berman, D.; Deshmukh, S. A.; Sankaranarayanan, S. K. R. S.; Erdemir, A.; Sumant, A. V. Macroscale Superlubricity Enabled by Graphene Nanoscroll Formation. *Science* **2015**, *348*, 1118–1122.
- (10) Wang, A. Y.; Lee, K. R.; Ahn, J. P.; Han, J. H. Structure and Mechanical Properties of W Incorporated Diamond-Like Carbon Films Prepared by a Hybrid Ion Beam Deposition Technique. *Carbon* **2006**, *44*, 1826–1832.
- (11) Wang, S.; Zhang, K.; An, T.; Hu, C. Q.; Meng, Q. N.; Ma, Y. Z.; Wen, M.; Zheng, W. T. Structure, Mechanical and Tribological Properties of HfC_x Films Deposited by Reactive Magnetron Sputtering. *Appl. Surf. Sci.* **2015**, *327*, 68–76.
- (12) Zhang, K.; Wen, M.; Meng, Q. N.; Hu, C. Q.; Li, X.; Liu, C.; Zheng, W. T. Effects of Substrate Bias Voltage on the Microstructure, Mechanical Properties and Tribological Behavior of Reactive

- Sputtered Niobium Carbide Films. *Surf. Coat. Technol.* **2012**, *212*, 185–191.
- (13) Liu, X.; Yang, J.; Hao, J.; Zheng, J.; Gong, Q.; Liu, W. A Near-Frictionless and Extremely Elastic Hydrogenated Amorphous Carbon Film with Self-Assembled Dual Nanostructure. *Adv. Mater.* **2012**, *24*, 4614–4617.
- (14) Chen, X.; Zhang, C.; Kato, T.; Yang, X. A.; Wu, S.; Wang, R.; Nosaka, M.; Luo, J. Evolution of Triboro-Induced Interfacial Nanostructures Governing Superlubricity in a-C:H and a-C:H:Si Films. *Nat. Commun.* **2017**, *8*, 1675.
- (15) Shi, J.; Wang, Y.; Gong, Z.; Zhang, B.; Wang, C.; Zhang, J. Nanocrystalline Graphite Formed at Fullerene-Like Carbon Film Frictional Interface. *Adv. Mater. Interfaces* **2017**, *4*, 1601113.
- (16) Shi, J.; Gong, Z.; Wang, Y.; Gao, K.; Zhang, J. Friction and Wear of Hydrogenated and Hydrogen-Free Diamond-Like Carbon Films: Relative Humidity Dependent Character. *Appl. Surf. Sci.* **2017**, *422*, 147–154.
- (17) Tripathi, K.; Gyawali, G.; Lee, S. W. Graphene Coating Via Chemical Vapor Deposition for Improving Friction and Wear of Gray Cast Iron at Interfaces. *ACS Appl. Mater. Interfaces* **2017**, *9*, 32336–32351.
- (18) Liao, Y.; Hoffman, E.; Wimmer, M.; Fischer, A.; Jacobs, J.; Marks, L. CoCrMo Metal-on-Metal Hip Replacements. *Phys. Chem. Chem. Phys.* **2013**, *15*, 746–756.
- (19) Liao, Y.; Pourzal, R.; Wimmer, M. A.; Jacobs, J. J.; Fischer, A.; Marks, L. D. Graphitic Tribological Layers in Metal-on-Metal Hip Replacements. *Science* **2011**, *334*, 1687–1690.
- (20) Kocijan, A.; Milošev, I.; Pihlar, B. The Influence of Complexing Agent and Proteins on the Corrosion of Stainless Steels and Their Metal Components. *J. Mater. Sci.: Mater. Med.* **2003**, *14*, 69–77.
- (21) Erdemir, A.; Ramirez, G.; Eryilmaz, O. L.; Narayanan, B.; Liao, Y.; Kamath, G.; Sankaranarayanan, S. K. R. S. Carbon-Based Tribofilms from Lubricating Oils. *Nature* **2016**, *536*, 67.
- (22) He, J. L.; Setsuhara, Y.; Shimizu, I.; Miyake, S. Untitledstructure Refinement and Hardness Enhancement of Titanium Nitride Films by Addition of Copper. *Surf. Coat. Technol.* **2001**, *137*, 38–42.
- (23) Gulbiński, W.; Suszko, T. Thin Films of Mo₂N/Ag Nanocomposite—the Structure, Mechanical and Tribological Properties. *Surf. Coat. Technol.* **2006**, *201*, 1469–1476.
- (24) Blanco, D.; González, R.; Hernández Battez, A.; Viesca, J. L.; Fernández-González, A. Use of Ethyl-Dimethyl-2-Methoxyethylammonium Tris (Pentafluoroethyl) Trifluorophosphate as Base Oil Additive in the Lubrication of TiN PVD Coating. *Tribol. Int.* **2011**, *44*, 645–650.
- (25) Lorenzo-Martin, C.; Ajayi, O. O.; Torrel, S.; Shareef, I.; Fenske, G. R. Friction and Wear Behavior of Thin-Film Ceramic Coatings under Lubricated Sliding Contact. *Thin Solid Films* **2014**, *569*, 70–75.
- (26) Liu, C.; Song, X.; Li, Q.; Ma, Y. M.; Chen, C. F. Smooth Flow in Diamond: Atomistic Ductility and Electronic Conductivity. *Phys. Rev. Lett.* **2019**, *123*, 195504.
- (27) Tung, H. M.; Huang, J. H.; Tsai, D. G.; Ai, C. F.; Yu, G. P. Hardness and Residual Stress in Nanocrystalline ZrN Films: Effect of Bias Voltage and Heat Treatment. *Mater. Sci. Eng., A* **2009**, *500*, 104–108.
- (28) Ma, S. L.; Ma, D. Y.; Guo, Y.; Xu, B.; Wu, G. Z.; Xu, K. W.; Chu, P. K. Synthesis and Characterization of Super Hard, Self-Lubricating Ti–Si–C–N Nanocomposite Coatings. *Acta Mater.* **2007**, *55*, 6350–6355.
- (29) Wang, D. S.; Chang, S. Y.; Huang, Y. C.; Wu, J. B.; Lai, H. J.; Leu, M. S. Nanoscopic Observations of Stress-Induced Formation of Graphitic Nanocrystallites at Amorphous Carbon Surfaces. *Carbon* **2014**, *74*, 302–311.
- (30) Robertson, J. Diamond-Like Amorphous Carbon. *Mater. Sci. Eng., R* **2002**, *37*, 129–281.
- (31) Dai, L.; Sorkin, V.; Zhang, Y. W. Effect of Surface Chemistry on the Mechanisms and Governing Laws of Friction and Wear. *ACS Appl. Mater. Interfaces* **2016**, *8*, 8765–8772.
- (32) Sun, C. Q.; Tay, B. K.; Lau, S. P.; Sun, X. W.; Zeng, X. T.; Li, S.; Bai, H. L.; Liu, H.; Liu, Z. H.; Jiang, E. Y. Bond Contraction and Lone Pair Interaction at Nitride Surfaces. *J. Appl. Phys.* **2001**, *90*, 2615–2617.
- (33) Zheng, W. T.; Sun, C. Q. Electronic Process of Nitriding: Mechanism and Applications. *Prog. Solid State Chem.* **2006**, *34*, 1–20.
- (34) Oktay, S.; Kahraman, Z.; Urgen, M.; Kazmanli, K. XPS Investigations of Tribolayers Formed on TiN and (Ti,Re)N Coatings. *Appl. Surf. Sci.* **2015**, *328*, 255–261.
- (35) Gunawan, C.; Teoh, W. Y.; Marquis, C. P.; Lifia, J.; Amal, R. Reversible Antimicrobial Photoswitching in Nanosilver. *Small* **2009**, *5*, 341–344.
- (36) Azimi, G.; Dhiman, R.; Kwon, H. M.; Paxson, A. T.; Varanasi, K. K. Hydrophobicity of Rare-Earth Oxide Ceramics. *Nat. Mater.* **2013**, *12*, 315–320.
- (37) Khan, S.; Azimi, G.; Yildiz, B.; Varanasi, K. K. Role of Surface Oxygen-to-Metal Ratio on the Wettability of Rare-Earth Oxides. *Appl. Phys. Lett.* **2015**, *106*, 061601.
- (38) Sattler, J. J.; Ruiz-Martinez, J.; Santillan-Jimenez, E.; Weckhuysen, B. M. Catalytic Dehydrogenation of Light Alkanes on Metals and Metal Oxides. *Chem. Rev.* **2014**, *114*, 10613–10653.
- (39) Reddy, B. M.; Khan, A. Recent Advances on TiO₂-ZrO₂ Mixed Oxides as Catalysts and Catalyst Supports. *Catal. Rev.: Sci. Eng.* **2005**, *47*, 257–296.
- (40) Sriprabha, D.; Mohankumar, T.; Nataraj, D.; Thangadurai, T. D. Enhanced Methylene Blue Dye Degradation by Newly Synthesized Ag₂O/TiO₂ Heterostructure. *J. Environ. Nanotechnol.* **2014**, *3*, 105–111.
- (41) Kumar, R.; El-Shishtawy, R.; Barakat, M. Synthesis and Characterization of Ag-Ag₂O/TiO₂@Polypyrrole Heterojunction for Enhanced Photocatalytic Degradation of Methylene Blue. *Catalysts* **2016**, *6*, 76.
- (42) Bowden, F. P.; Ridler, K. E. W. Physical Properties of Surfaces - III—the Surface Temperature of Sliding Metals - the Temperature of Lubricated Surfaces. *Proc. R. Soc. A* **1936**, *154*, 640–656.
- (43) Rappe, A. K.; Goddard, W. A., III Charge Equilibration for Molecular Dynamics Simulations. *J. Phys. Chem.* **1991**, *95*, 3358–3363.
- (44) van Duin, A. C. T.; Dasgupta, S.; Lorant, F.; Goddard, W. A. Reaxff: A Reactive Force Field for Hydrocarbons. *J. Phys. Chem. A* **2001**, *105*, 9396–9409.
- (45) Ren, P.; Zhang, K.; He, X.; Du, S. X.; Yang, X.; An, T.; Wen, M.; Zheng, W. T. Toughness Enhancement and Tribocorrosion of the Nb-Ag-N Films Actuated by Solute Ag. *Acta Mater.* **2017**, *137*, 1–11.
- (46) Zhao, Y.; Liu, J.; Zhao, Y.; Wang, F.; Song, Y. Pt-Co Secondary Solid Solution Nanocrystals Supported on Carbon as Next-Generation Catalysts for the Oxygen Reduction Reaction. *J. Mater. Chem. A* **2015**, *3*, 20086–20091.
- (47) Ren, P.; Zhang, K.; Du, S. X.; Zhao, Z.; Wen, M.; Zheng, W. T. Achieving Highly Hydrophobic or Hydrophilic HfN_x-Ag Films Surfaces by Controlling the Existing Forms of Ag. *Mater. Lett.* **2017**, *207*, 161–164.
- (48) Ren, P.; Zhang, K.; Du, S. X.; Meng, Q. N.; He, X.; Wang, S.; Wen, M.; Zheng, W. T. Tailoring the Surface Chemical Bond States of the NbN Films by Doping Ag: Achieving Hard Hydrophobic Surface. *Appl. Surf. Sci.* **2017**, *407*, 434–439.
- (49) Bachmann, S.; Fielenbach, D.; Jorgensen, K. A. Cu(I)-Carbenoid - and Ag(I)-Lewis Acid-Catalyzed Asymmetric Intermolecular Insertion of Alpha-Diazo Compounds into N-H Bonds. *Org. Biomol. Chem.* **2004**, *2*, 3044–3049.
- (50) Tian, Q.; Shi, D.; Sha, Y. CuO and Ag₂O/CuO Catalyzed Oxidation of Aldehydes to the Corresponding Carboxylic Acids by Molecular Oxygen. *Molecules* **2008**, *13*, 948–957.
- (51) Fridman, V. Z.; Xing, R. Investigating the CrO_x/Al₂O₃ Dehydrogenation Catalyst Model: II. Relative Activity of the Chromium Species on the Catalyst Surface. *Appl. Catal., A* **2017**, *530*, 154–165.
- (52) Tian, Y. P.; Bai, P.; Liu, S. M.; Liu, X. M.; Yan, Z. F. VO_x-K₂O/γ-Al₂O₃ Catalyst for Nonoxidative Dehydrogenation of Isobutane. *Fuel Process. Technol.* **2016**, *151*, 31–39.

Electronic Supplementary Information

for

Ultralow-Friction and Ultralow-Wear TiN-Ag Solid Solution Coating in Base-Oil

Chang Liu[†], Xinlei Gu[†], Lina Yang[†], Xianqi Song[†], Mao Wen[†], Jia Wang[†], Quan Li[†], Kan Zhang^{*,†}, Weitao Zheng^{*,†} and Changfeng Chen^{*,‡}

[†]State Key Laboratory of Superhard Materials, Department of Materials Science and Key Laboratory of Automobile Materials, MOE, Jilin University, Changchun 130012, China.

[‡]Department of Physics and Astronomy, University of Nevada, Las Vegas, Nevada 89154, USA

*Kan Zhang. E-mail: kanzhang@jlu.edu.cn

*Weitao Zheng. E-mail: wtzheng@jlu.edu.cn

*Changfeng Chen. E-mail: chen@physics.unlv.edu

This supporting file includes:

- The details of sample preparation, characterization, AIMD simulations
- Supporting Table S1
- Supporting Figure S1-S8
- Supporting references

Methods

Sample Preparation

TiN coatings with solute Ag atoms were deposited on Si(100) substrates by magnetron co-sputtering individual Ti (99.95%) and Ag (99.99%) targets in mixed discharge gases of Ar (99.999 %) and N₂ (99.999 %). For comparison, coatings of pure TiN and TiN with precipitated Ag clusters were also prepared. Before deposition, all substrates were ultrasonically cleaned in subsequent baths of acetone, alcohol and deionized water for 15 min, blown dry with dry nitrogen. Base pressure lower than 5×10^{-4} Pa was achieved using a turbo molecular pump, then a mixture of Ar/N₂ (65/20 sccm) was introduced to generate a working pressure of 0.8 Pa. For deposition of TiN coatings, a high bias voltage at -130 V was applied during sputtering to create high internal stresses. To regulate different forms of Ag (solute or precipitated state), a direct current of 0.55 A (190 W) and radio frequency powers of 15 and 30 W, respectively, were linked to Ti and Ag target. No additional heat source was applied during deposition, and substrate temperature was about 100 °C throughout this process. Target-substrate distance and substrate rotational speed were fixed at 80 mm and 10 r/min, respectively. A Ti interlayer of about 200 nm in thickness was first deposited to enhance the adhesion of all coatings. In addition, we also prepared Ag₂O and TiO₂ films on Si (001) substrates using Ti (99.95%) and Ag (99.99%) targets for tribological tests to examine catalytic capability. To obtain Ag₂O and TiO₂ films, different direct currents of 0.25 A (100W) and 0.23 A (100W) were linked to the Ag and Ti targets, respectively, and the working pressure was fixed at 0.8 Pa in the Ar/O₂ mixture (40sccm/40sccm and 78sccm/2sccm, respectively). Other deposition parameters were the same as for Ag containing TiN film.

Characterization

Surface bonding states were characterized by X-ray photoelectron spectroscopy (XPS, ESCALAB-250) using Al K α as the X-ray source at 2 keV energy. To determine accurate coating composition through this measurement, all samples were etched with

Ar ion beam for 5 min in advance to remove surface oxides. A structural analysis was done by a combination of X-ray diffraction with monochromatized Cu K α radiation (XRD, D8-tools) and high-resolution transmission electron microscopy (HRTEM, JEOL 2010F) operated at 200-kV accelerate voltage. The measurements of lattice spacing were performed using the DiffTools suite in DigitalMicrograph software¹. The thickness and curvatures radius for the samples were measured by the surface profiler (Veeco Dektak 150), taking a minimum of six measurements along two orthogonal surface directions, and the total residual stress was obtained using the Stoney equation.² Surface morphology and root-mean-square roughness (R_q) were obtained using Dimension Icon atomic force microscope (AFM). For the measurement of mechanical properties, MTS Nanoindenter XP equipped with continuous stiffness measurements mode³ was used to evaluate hardness, with the stiffness monitored continuously during the loading of the indenter by imposing a small dynamic oscillation on the displacement signal and measuring the amplitude and phase of the corresponding force signal by means of a frequency-specific amplifier. During the test, a Berkovitch-type pyramidal diamond tip was chosen to indent the film to a penetration depth of 1,000 nm, simultaneously obtaining stiffness results by oscillating the tip during indentation with a frequency of 45 Hz and amplitude of a few nanometers. For each test, at least six indentations at different places on the film surface were made. Measured results from a penetration depth range of 100-200 nm was considered to estimate the true hardness of deposited coatings to minimize the surface and substrate effects. Tribological behaviors were tested on a CSM ball-on-disk tribometer in ambient environment (room temperature, ~35 % relative humidity) under oil lubricated sliding condition, where 0.05 ml PAO 10 oil (kinematic viscosity is 70 mm²/s at 40 °C), measured by a 1 ml syringe, was applied to the sliding contact surface to cover the whole rubbing surface. Al₂O₃ balls in 6 mm diameter were used as sliding counterparts. The tests for TiN and Ag-containing TiN samples were performed under a 5-N load with a sliding velocity of 5 cm/s, and the total sliding cycles were set at 10,000. After the tests, all the samples were ultrasonically cleaned in acetone for 10 min to wipe off the oil on the coating surface, and then wear track profiles were observed by 3D Laser Confocal Scanning

Microscope (OLLYMPUS 2EXT) to examine wear conditions. Wear trace cross sections of all coatings were characterized by means of surface profiler (Veeco Dektak 150). Subsequently, wear rates for coatings were determined by assessing the average wear volume per sliding distance per normal load. Besides, the surface appearance and element distribution of wear trace for each sample was also characterized by scanning electron microscopy (SEM, JEOL JSM-6700F) equipped with an energy dispersive x-ray spectroscopy (EDS) module. The chemical nature of generated debris on the counterpart ball was identified by Raman analysis (HORIBA-T64000) under 514.5 nm excitation. TEM measurements were carried out to further examine structural features. The whole ball with both residual oil and wear debris was ultrasonically cleaned in ethanol for 20 min, then centrifugation for liquid and solid debris was done by ZONKIA high speed centrifuge (HC-3018) with a rotate speed of 10,000 r/min for 10 min. Subsequently, we discarded supernatant liquid and dispersed the rest with alcohol in ultrasonic bath. The samples on Cu grids for TEM analysis were transferred from the dispersed liquid mixture with a dropper. Water contact angle (WCA) was evaluated using a Krus-DSA30 device to detect and verify formation of surface oxides. To explore mechanisms for observed catalytic effects, oxides samples (Ag_2O and TiO_2) were also examined by tribological tests, with the load, sliding velocity and total sliding cycles set at 1N, 3 cm/s and 10,000 cycles, respectively. The chemical nature of wear debris on the rapping ball was also characterized by Raman analysis (HORIBA-T64000) under 514.5 nm excitation. The element concentration at the sample surfaces of Ag_2O and TiO_2 was measured by SEM (JEOL JSM-6700F) equipped with EDS modules.

AIMD simulations

Ab-initio molecular dynamics (AIMD) simulations in the canonical ensemble (NVT) were conducted to assess catalytic capability of TiN coating films with different amount and form of Ag contents. The exchange correlation described by the Perdew-Burke-Ernzerhof (PBE) functional⁴, and the generalized gradient approximation (GGA) using the projector-augmented wave formalism as implemented in the Vienna Ab-initio

Simulation Package (VASP)^{5,6} were employed. The plane wave energy cut-off is set at 520 eV. The Brillouin zone is sampled at the Γ -point. We monitored the temporal evolution of 1-pentene molecule on four different surfaces: Ag (111), TiN (111), TiO₂ (110), Ag₂O (110) and at a constant temperature 1,000 K for 400 fs using a timestep of 0.5 fs. The pentene molecule is initially placed at a random location on each surface. The surface slab supercells comprise 5 atomic layers with dimensions about 1.5 nm x 1.5 nm in the plane of each layer. A vacuum of 2 nm was employed in the direction normal to the surface. Periodic boundary conditions are employed along all directions.

Table S1. Experimental parameters (input power of Ti/Ag target), composition, hardness H , elastic modulus E , residual internal stress IS , and the calculated formation enthalpy ΔH (eV/atom) for samples numbered in order of Ag target sputtering power.

Sample	Ti/Ag (W)	Composition (at.%)			H (GPa)	E (GPa)	IS (-GPa)	ΔH^* (eV/atom)
		Ti	N	Ag				
1	190/0	52.9	47.1	0	33.9 ± 2.2	309.8 ± 9.0	5.16	-1.692
2	190/15	50.1	47.2	2.7	39.6 ± 3.1	314.5 ± 6.5	5.15	-1.472
3	190/30	45.2	41.2	13.6	10.6 ± 2.3	119.6 ± 10.8	0.15	-

*Calculated enthalpy values are obtained using the VASP code under the GGA.

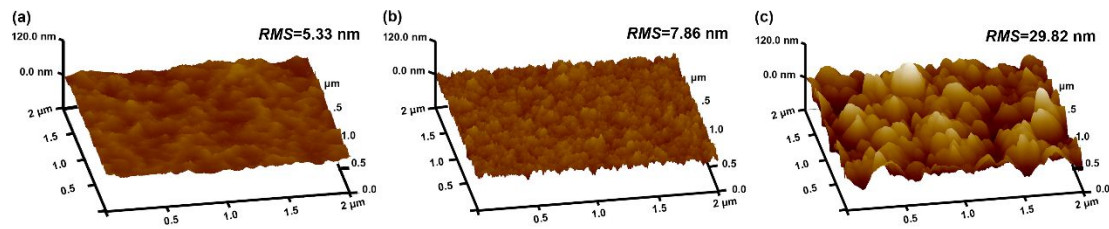


Figure S1. AFM 3D images in dimensions of $2 \times 2 \mu\text{m}^2$, in which the root-mean-square (*RMS*) roughness is marked, and all ordinates for sample height are normalized to -120~120 nm.

Atomic force microscope (AFM) measurements provide an accurate description on the morphology of synthesized film layers. Experimental results presented above reveal that the pure TiN coating possesses a rather flat surface with a small root-mean-square (*RMS*) roughness value of 5.33 nm (Fig. S1a), and the same is seen in the TiN film with 2.7 at.% Ag (Fig. S1b) that has a similarly small *RMS* roughness value of 7.86 nm. In stark contrast, the TiN film with 13.6 at.% Ag (Fig. S1c) exhibits large protuberances that are clearly visible in the 3D image, with a greatly increased *RMS* roughness value of 29.82 nm. Such large variations in *RMS* roughness values indicate a strong influence of precipitated Ag nanoclusters on the morphology of the synthesized TiN film.

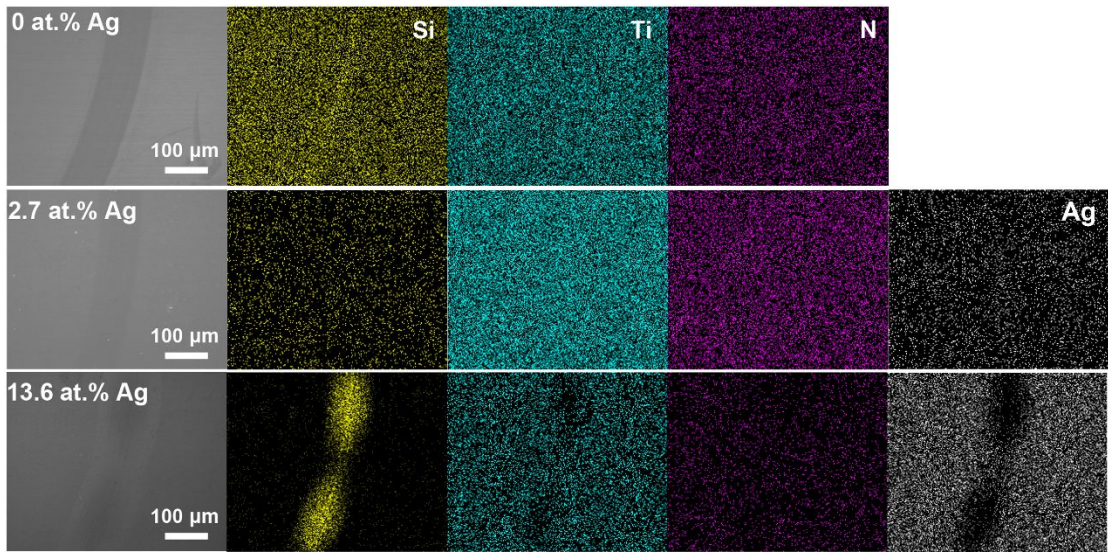


Figure S2. SEM micrographs and SEM-EDS mapping images on worn surfaces for the samples with 0 at.% Ag (top row), 2.7 at.% Ag (middle row) and 13.6 at.% Ag (bottom row).

The scanning electron microscopy (SEM) with an energy dispersive x-ray spectroscopy (EDS) mapping is an effective characterization tool to record and display the degree of wear. In the figure above (Fig. S2) we present the appearance and element distribution of wear trace for pure TiN and Ag-containing TiN samples. An un-sharpness Si element enriched area (yellow color) is observed in the wear trace of the pure TiN film, which corresponds to a slight wear. Meanwhile, wear condition is considerably worse for TiN-Ag film with 13.6 at.% Ag, which exhibits a large Si element enriched area, indicating a severely worn condition. In contrast, no apparent wear trace can be detected for the TiN-Ag film with 2.7 at.% Ag, which shows the dimmest, practically invisible Si signal.

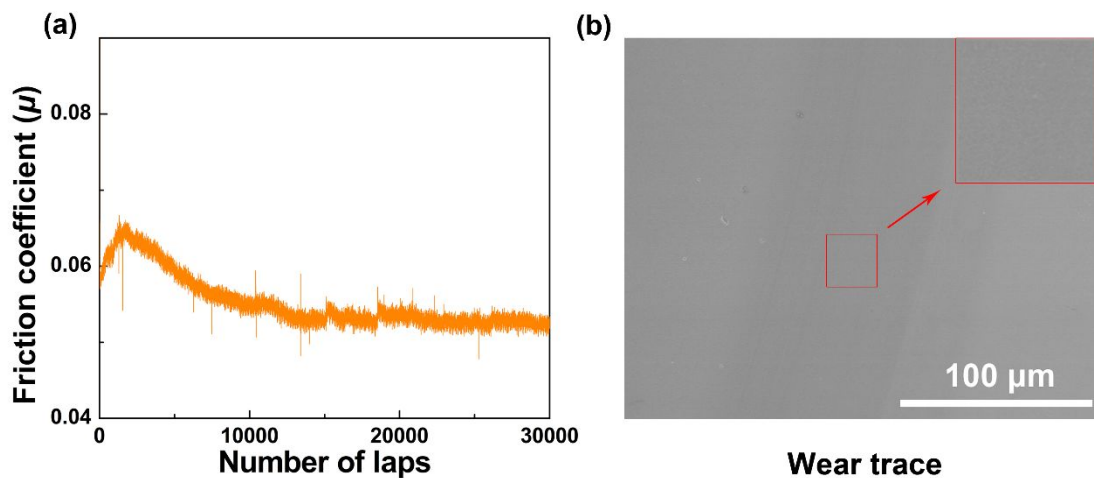


Figure S3. (a) The friction curve of TiN-Ag solid solution coating as a function of sliding cycle; (b) The surface morphology of wear traces for TiN-Ag solid solution coating after 30,000 cycles.

Figure S3(a) presents the friction curves for the TiN-Ag solid solution coating as a function of sliding cycle. The sample in the long friction process retains the low and stable friction coefficient that is similar to the results from the 10,000 cycles. The wear traces for the TiN-Ag solid solution sample were characterized by SEM and plotted in Figure S3(b), which shows smooth wear trace on TiN-Ag solid solution coating, with no cracks on the wear trace, indicating the high toughness of the sample.

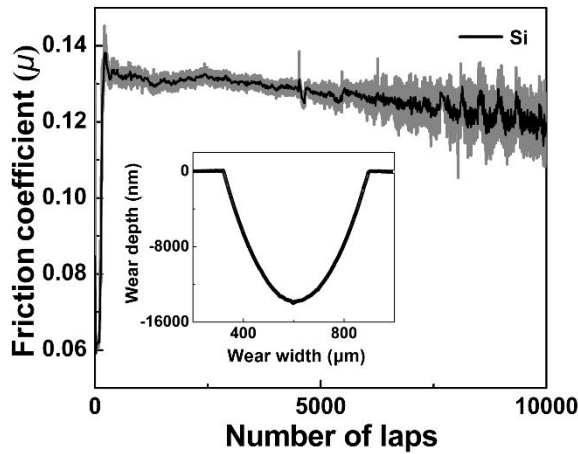


Figure S4. Friction coefficient (μ) for an uncoated Si substrate against an Al_2O_3 ball under base-oil lubricated condition as a function of sliding cycle. The wear condition of the uncoated Si substrate is shown in the inset.

For comparison, an uncoated Si substrate was tested in the same friction condition as the deposited coatings (see Fig. 2b). As shown in Fig. S4, the pure Si substrate under the base-oil lubricated condition exhibits rather high μ values around 0.122, and the measured results become very unsteady at increasing test laps. This phenomenon is attributed to the presence of mass of wear-related debris particles generated and accumulated at the sliding-contact interface, which were caused by severe wear losses of the substrate. To confirm this inference, the wear depth of the uncoated Si substrate was measured by a surface profiler, and the results shown in the inset of Fig. S4 allows a computation of the wear rate as high as $1.04 \times 10^{-7} \text{ mm}^3/\text{Nm}$, which is three orders of magnitude higher than the value for the TiN-Ag solid solution coating.

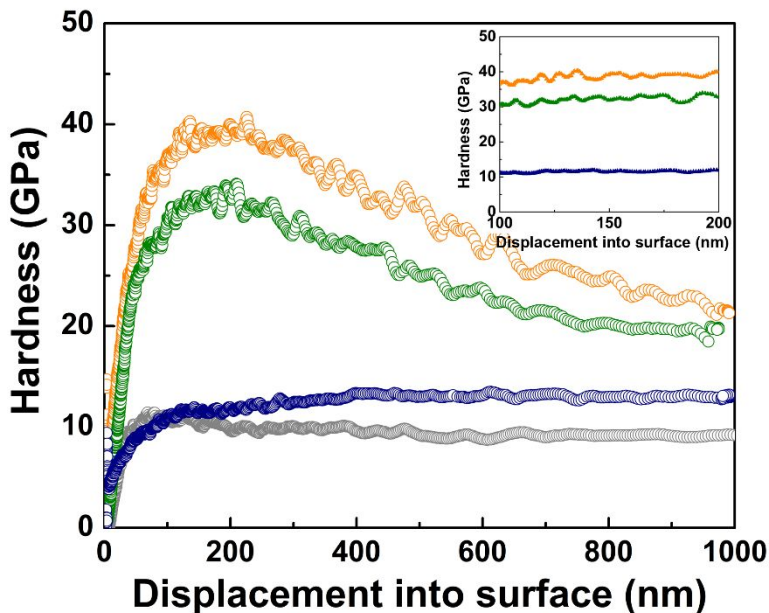


Figure S5. Hardness (H) for TiN-Ag films and fused silica sample as a function of displacement into the test surface. Results in the depth range most suitable for assessing the intrinsic hardness of TiN-Ag films are shown in the inset.

To characterize mechanical properties and corroborate observed anti-wear features, we have measured indentation hardness (H) of the TiN-Ag films and compared the results against that of the fused silica standard sample. In Fig. S5 we present the measured hardness data as a function of indentation depth. The standard sample exhibits a steady value at approximately 10 GPa with indentation depth increasing from 50 nm to the maximum depth, preceded by a quick initial rise due to the surface effect. Similar patterns are also observed in the TiN-Ag film coatings, where the measured hardness values are further influenced by Si substrates at deeper indentation depths (> 200 nm). We have taken intrinsic hardness values at an impression depth range of 100-200 nm to minimize the effects from both the surface⁷ and the substrate.⁸

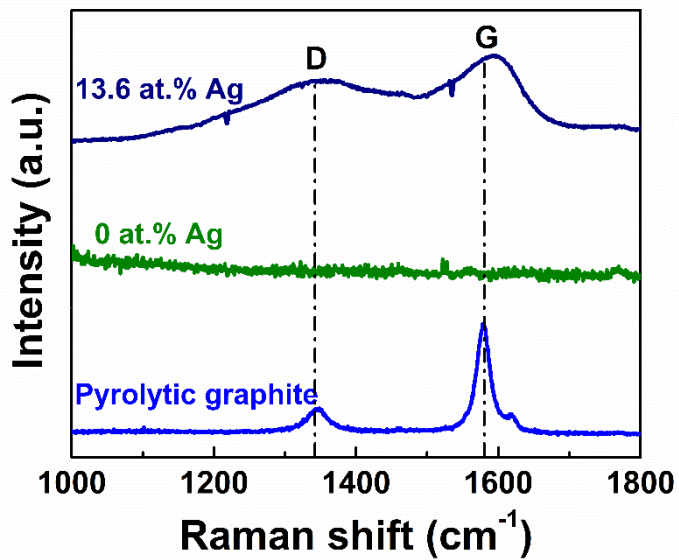


Figure S6. Raman signal of friction debris on the Al_2O_3 ball for the cases where the coatings have Ag content of 0 at.% and 13.6 at.%, respectively. The pyrolytic graphite was chosen as reference.

Besides the TiN-Ag solid solution sample, Raman test was also performed on friction debris on Al_2O_3 balls for the pure TiN sample and TiN-Ag sample with 13.6 at.% Ag. Results in the above figure (Fig. S6) clearly show that friction debris from the TiN-Ag sample with 13.6 at.% Ag displays obvious D and G peaks, which are similar to the results for the previously reported $\text{MoN}_x\text{-Cu}$ coating. In contrast, no such Raman signal was detected in friction debris from the pure TiN sample, indicating that no graphite has been formed by this sample during the sliding test.

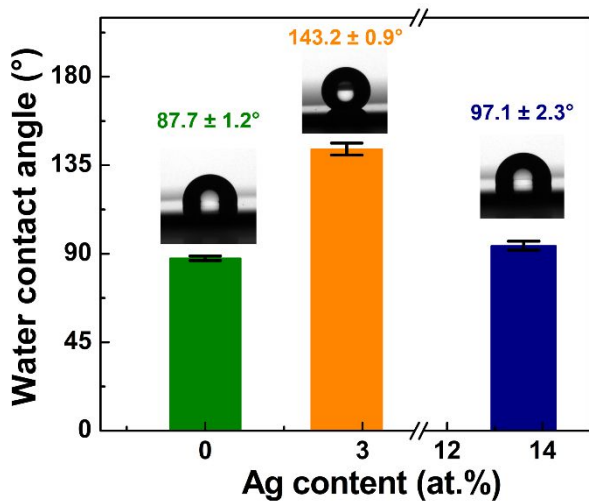


Figure S7. The water contact angles (WCA) on the TiN-Ag coating films with different Ag contents.

Figure S7 shows the variation of water contact angles (WCA) on three TiN-Ag coating films with different Ag contents. The pure TiN coating exhibits low WCA at $87.7 \pm 1.2^\circ$ (below 90°); incorporating 2.7 at.% Ag atoms drastically raises WCA to $143.2 \pm 0.9^\circ$ to achieve high hydrophobicity (approaching the superhydrophobicity WCA of 150°); but excessive Ag content at 13.6 at.% lowers the WCA to $97.1 \pm 2.3^\circ$.

Generally, the wettability of a solid surface can be controlled by surface energy, which depends on the surface chemical state. In particular, a special electronic state with filled-shell structure is expected to have little tendency to interact with water molecules, thus facilitating the achievement of hydrophobicity. In this study, the Ag^+ in Ag_2O is coordination saturated with a filled-shell ($4\text{d}^{10}\text{S}^0$) structure, thus the coating with high hydrophobicity induced by solute Ag atoms should possess the most Ag_2O concentration (i.e., the strongest self-oxidation ability), confirming the XPS results presented in Figs. 4a and 4b in the main text.

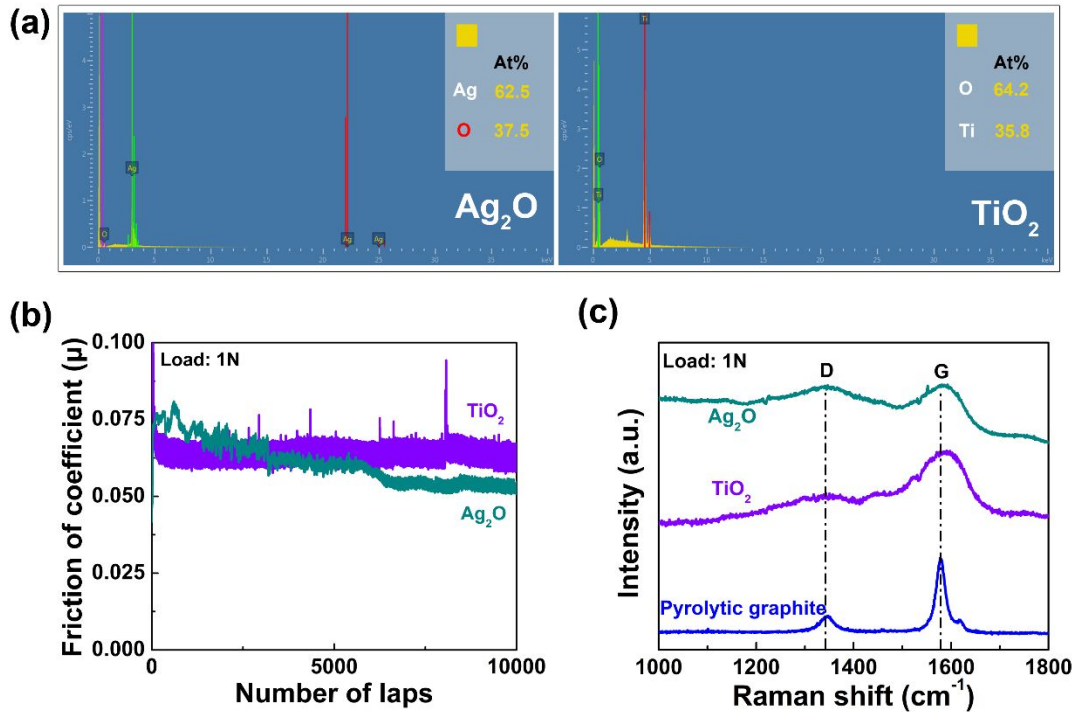


Figure S8. The (a) EDS, (b) friction coefficient and (c) Raman spectra for the Ag_2O and TiO_2 coatings.

To examine the catalytic capability of Ag and Ti oxides, we deposited Ag_2O and TiO_2 coatings on Si (001) substrates, and carried out tribological tests under 1N loads. The resulting wear traces were characterized by Raman analysis. After deposition, the obtained oxide coatings were first examined by EDS results to verify the composition, and the results are presented in Fig. S8a, which show clearly that $\text{Ag}_{62.5}\text{O}_{37.5}$ and $\text{Ti}_{35.8}\text{O}_{64.2}$ coatings were successfully prepared, and the Ag/O and Ti/O atomic ratios were close to 2/1 and 1/2, respectively. Subsequently, these nominally Ag_2O and TiO_2 coatings were studied by tribological tests in 0.05 ml PAO 10 oil. The sliding counterpart, sliding velocity and total sliding cycles were chosen to be Al_2O_3 ball, 3 cm/s and 10,000 cycles, respectively. Results in Fig. S8b show that friction coefficients were stable at 0.050 and 0.063, respectively. After the tribological tests, friction debris on the wear trace was characterized by Raman analysis. Results in Fig. S8c show that the wear trace for both Ag_2O and TiO_2 coatings exhibited clear D and G peaks, meaning that both of these oxides possess catalytic capability to extract graphitic tribofilms from lubricating PAO oil. These findings strongly corroborate results of AIMD simulations.

References

- (1) Mitchell, D. R. G. DiffTools: Electron Diffraction Software Tools for DigitalMicrograph™, *Microsc. Res. Tech.* **2008**, *71*, 588-593.
- (2) Zhang, K.; Wen, M.; Cheng, G.; Li, X.; Meng, Q. N.; Lian, J. S.; Zheng, W. T. Reactive Magnetron Sputtering Deposition and Characterization of Niobium Carbide Films, *Vacuum* **2014**, *99*, 233-241.
- (3) Li, X.; Bhushan, B. A Review of Nanoindentation Continuous Stiffness Measurement Technique and Its Applications, *Mater. Charact.* **2002**, *48*, 11-36.
- (4) Perdew, J. P.; Burke, K.; Ernzerhof, M. Generalized Gradient Approximation Made Simple, *Phys. Rev. Lett.* **1996**, *77*, 3865.
- (5) Kresse, G.; Furthmüller, J. Efficient Iterative Schemes for Ab Initio Total-Energy Calculations Using a Plane-Wave Basis Set, *Phys. Rev. B* **1996**, *54*, 11169.
- (6) Kresse, G.; Furthmüller, J. Efficiency of Ab-Initio Total Energy Calculations for Metals and Semiconductors Using a Plane-Wave Basis Set, *Comp. Mater. Sci.* **1996**, *6*, 15-50.
- (7) Bobji, M. S.; Biswas, S. K.; Pethica, J. B. Effect of Roughness on the Measurement of Nanohardness—a Computer Simulation Study, *Appl. Phys. Lett.* **1997**, *71*, 1059-1061.
- (8) Li, X.; Gao, H.; Murphy, C. J.; Caswell, K. K. Nanoindentation of Silver Nanowires, *Nano Lett.* **2003**, *3*, 1495-1498.
- (9) Wang, H.; Yu, J.; Wu, Y.; Shao, W.; Xu, X. A Facile Two-Step Approach to Prepare Superhydrophobic Surfaces on Copper Substrates, *J. Mater. Chem. A* **2014**, *2*, 5010-5017.